Wastewater Hydraulics

Theory and Practice

Bearbeitet von
Willi H. HAGER

2nd Edition. 2010. Buch. xx, 652 S. Hardcover
ISBN 978 3 642 11382 6
Format (B x L): 15,5 x 23,5 cm
Gewicht: 2460 g

Chapter 2
Losses in Flow

Abstract Flow losses take place either as friction loss due to wall friction and viscosity or as local flow loss depending on conduit or channel geometry. Both types of losses are described in detail for conduit flow.

The *friction losses* are given by the transition law developed by Colebrook and White and by the solution of the equation of Gauckler-Manning-Strickler. The application criteria of the two formulae are given and the roughness values are presented in tables.

The *local losses* are ascertained for a number of conduit geometries and channel configurations and optimal dimensional ratios are indicated. Finally, flows in pressure conduits and free-surface channels are compared.

2.1 Introduction

It is a well-known fact that mechanical processes are always accompanied by the dissipation phenomenon. It is not possible, therefore, to maintain the initial energy over a certain temporal duration or a local distance without spending additional energy, because these motions are accompanied by physical transformation into thermal energy. One speaks therefore of *energy loss* (German: Energieverlust; French: Perte de charge), whereby only the loss relative to the original mechanical energy is considered.

In hydraulics two kinds of energy losses are distinguished in principle. On the one hand there are losses owing to wall boundaries, referred to as the *boundary layer* and having close causal connection with the viscosity of the fluid and the condition of the wall. On the other hand losses also appear due to changes in the cross-section of the flow and in the direction of the motion. Whenever the flow accelerates or, in particular, decelerates, *separation* occurs and mechanical energy from the flow is withdrawn by large scale vortex motion.

The first kind of loss is closely associated with the boundary layer development and is designated, in accordance with the nomenclature of classical works, as *wall friction loss*. The second kind of loss is intimately linked with the flow geometry and is therefore designated as *form loss* or additional loss (additional to wall friction

W.H. Hager, *Wastewater Hydraulics*, 2nd ed., DOI 10.1007/978-3-642-11383-3_2,

loss). The friction loss is produced by shear stresses along the boundary walls and accounted for in the momentum equation, whereas the additional loss arises from internal shear stresses and may be determined only from indirect considerations.

In the following sections the two kinds of losses are treated individually. The *total loss* ΔH_g is defined as the sum of frictional (subscript R) and additional losses (subscript L for local) as

$$\Delta H_g = \Delta H_R + \Delta H_L. \tag{2.1}$$

Thus the hydraulic losses are estimated using the *principle of superposition*. This principle may naturally be applied with confidence only if the sources of the additional losses lie sufficiently apart. It is on this premise that the combining principle is accounted for.

2.2 Friction Losses

2.2.1 *Equation of Colebrook and White*

As already mentioned, the term "friction loss" is the current customary designation for a loss resulting from the boundary layer development. Although not quite correct, this expression has become popular and shall be so used here.

Consider first a very long cylindrical *pipe of circular cross-section* containing a liquid of constant temperature. Let, for this flow, the discharge be Q, the diameter of the pipe be D, the mean velocity $V = Q/(\pi D^2/4)$ and the kinematic viscosity be ν. If the friction loss is ΔH_R per elementary length Δx, then the *friction gradient* is designated as $S_f = \Delta H_R/\Delta x$. It follows, therefore, that S_f participates in the flow process as a dependent variable.

The English scientist Osborne Reynolds (1842–1912) established that the dimensionless number, which today bears his name,

$$\mathsf{R} = VD/\nu \tag{2.2}$$

essentially describes the *flow regime*. Guided by his experiments with various fluids, Reynolds showed that the *laminar*, i.e. the layered motion, passes into *turbulent* motion if a Reynolds number of about 2300 is exceeded. For water of usual quality, corresponding to about 10°C, the transition velocity (subscript t) is about $V_t = 2{\cdot}10^{-3}$ ms^{-1} for $D = 1$ m. Thus, in hydraulic practice, *turbulent flow* appears almost exclusively.

The friction gradient S_f increases almost quadratically with the velocity head ($V^2/2g$) and decreases somewhat linearly with the pipe diameter D. These characteristics led both Henry Darcy (1803–1858) and Julius Weisbach (1806–1871) to propose

$$S_f = \frac{V^2}{2g} \cdot \frac{f}{D}, \tag{2.3}$$

where the so-called *friction factor* f (written as λ in German texts) must nearly be constant. Detailed measurements in the beginning of the twentieth century showed that f depends, essentially, on the *Reynolds number* R, as defined in Eq. (2.2), and the so called *relative wall roughness* $\varepsilon = k_s/D$. The parameter k_s here denotes the wall roughness height of a conduit which produces the same friction loss as is produced by a Nikuradse's sand-roughened pipe (Johann Nikuradse 1894–1979). The roughness measure is also described as the *equivalent sand roughness*.

The idea that a very complex surface irregularity of a conduit can be replaced by a well defined quantity is ingenious and was suggested by Ludwig Prandtl (1875–1953). The sand-roughened pipes were artificially pasted with uniform diameter sand grains and the losses resulting from experiments were measured. Each pair of values (R; ε) therefore yielded a value for the friction factor f. The preceding procedure was repeated for a pipe with arbitrary roughness matrix so that practically the same combination of parameters occurs although another pipe indicates an altogether different wall surface condition. Nevertheless, it would then possess an identical *relative sand roughness* for this discharge. The value of k_s varies in general with the discharge Q and consequently with R. The reason for this lies in the fact that sand-roughened and commercial pipes behave differently with regard to boundary layer development.

In the year 1937 the Englishmen Colebrook and White analyzed the results of experiments on turbulent flow in so-called *smooth pipes* (German: Glatte Rohre; French: Conduites lisses) for which the effect of the Reynolds number predominates, and *rough pipes* (German: Rauhe Rohre; French: Conduites rugueux) in which the parameter ε is of primary importance. For arbitrary turbulent conduit flows they developed a universal law for the friction factor f as a function of relative wall roughness $\varepsilon = k_s/D$ and the Reynolds number R. This *universal friction law* is given by the relation

$$\frac{1}{\sqrt{f}} = -2\log\left[\frac{\varepsilon}{3.7} + \frac{2.51}{\mathsf{R}\sqrt{f}}\right], \quad \mathsf{R} > 2300. \tag{2.4}$$

Figure 2.1 shows graphically the solution of Eq. (2.4) proposed by Moody (1880–1953) in his Moody diagram. One recognizes the various curves $f(\mathsf{R})$ which, depending on the relative roughness ε, approach asymptotically a particular value of f. The larger the value of ε, the higher is this level of f. In the *rough flow regime* there exists, for every relative roughness ε for $\mathsf{R}\to\infty$, a minimum value of the friction factor f. According to Eq. (2.4), the asymptotically approached minimum value of f is

$$f_{\min}^{-1/2} = -2\log(\varepsilon/3.7). \tag{2.5}$$

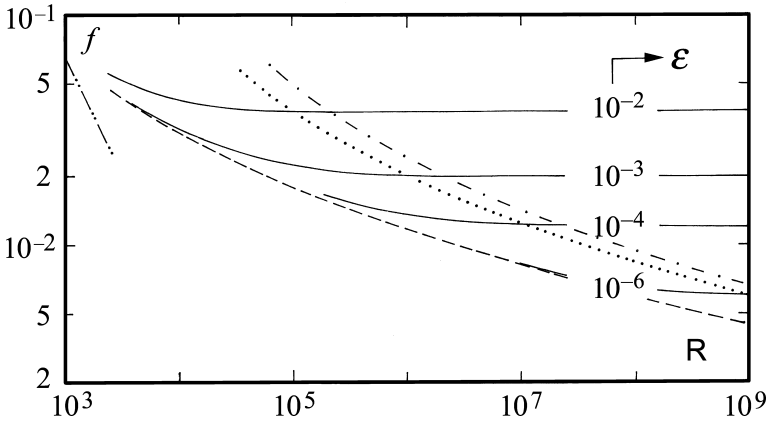

Fig. 2.1 Moody-Diagram, friction factor f as function of Reynolds number $\mathsf{R} = VD/\nu$ for various values of relative wall roughness $\varepsilon = k_s/D$ after Eq. (2.4). (-··· -) laminar flow, (- · -) 0.75% and (...) 1.5% deviation from fully developed turbulent flow

Hager (1987) observed a deviation in f from $f_{\min}$ of about 1.5% as the limit of the so-called *practical rough flow regime*. This yields, for the limiting relative roughness

$$\varepsilon_r = \frac{1050}{\mathsf{R}}. \tag{2.6}$$

If $\varepsilon > \varepsilon_r$, as is usually found in practice for flows in the rough regime, Eq. (2.5) is to be used. If, however, $\varepsilon < \varepsilon_r$ one has to fall back upon the generalized Eq. (2.4) of Colebrook and White.

In contrast to the rough regime, the flow in the *smooth flow regime* differs only insignificantly from the case $\varepsilon \to 0$. In this case the effect of the wall roughness becomes small in comparison to that of viscosity and one speaks of the *practical smooth flow regime* (subscript s). This is the case if $\varepsilon < \varepsilon_s$ with (Hager 1987)

$$\varepsilon_s = (3.475\mathsf{R})^{-0.9}. \tag{2.7}$$

The range $\varepsilon_s < \varepsilon < \varepsilon_r$ defines the turbulent *transition regime* (German: Übergangsregime; French: Régime de transition) for which the effects of both viscosity *and* wall roughness are to be considered.

Channel flows, in practice, usually take place under Reynolds numbers R in the range of values between 3×10^4 and 3×10^7 and relative roughnesses ε between 10^{-5} and 10^{-1}. Figure 2.1 shows that the 'smooth' flow regime is rather an unlikely phenomenon in practice. In the following only the transition regime and, particularly, the rough flow regime are considered.

2.2.2 *Transition Regime*

The flow processes in conduits of *circular cross-section* are described by five independent parameters:

- Friction gradient S_f,
- Discharge Q,
- Diameter D,
- Equivalent sand-roughness height k_s, and
- Kinematic viscosity ν.

In problems arising in practice, the determination of the first three parameters is relevant. Values of k_s and ν (Table 3.1) are known in advance.

For the *first type of problem*, the Reynolds number $\mathsf{R} = 4Q/(\pi\nu D)$ as well as the roughness characteristic $\varepsilon = k_s/D$ are known and f can be found either graphically from Fig. 2.1 or iteratively by Eq. (2.4). This implicit relation in f has also been approximated explicitly. For example, Zigrang and Sylvester (1985) proposed

$$f = \frac{1}{4}\left[\log\left(\frac{\varepsilon}{3.7} + \frac{13}{\mathsf{R}}\right)\right]^{-2}. \tag{2.8}$$

In the practical ranges of R and ε, the values of f calculated from Eq. (2.8) and those obtained from the Colebrook and White relationship differ only by about 2%. Other proposals (of explicit representation) have been explained by Chen (1985).

The *second type of problem*, in which the discharge Q is determined, can be solved explicitly by carrying out a transformation of Eq. (2.4) as

$$\hat{q} = Q/Q_o, \quad N = Q_o/(D\nu) \tag{2.9}$$

with $Q_o = (gS_fD^5)^{1/2}$ as the normalizing discharge. Substitution of these in Eq. (2.4) yields the discharge equation (Sinniger and Hager 1989)

$$\hat{q} = -\frac{\pi}{\sqrt{2}}\log\left[\frac{\varepsilon}{3.7} + \frac{2.51}{\sqrt{2}\,N}\right]. \tag{2.10}$$

Use of Eq. (2.10) is facilitated with Fig. 2.2.

The *third type of problem* is most frequently encountered in practice. It involves the determination of the pipe diameter D. For this, $(^*)$ denoted parameters are defined as

$$D^* = D/D_o, \quad k_s^* = k_s/D_o, \quad \nu^* = D_o\nu/Q \tag{2.11}$$

where $D_o = [Q^2/(gS_f)]^{1/5}$ and the unknown diameter D is separated. Introducing these dimensionless variables into Eq. (2.4) yields the implicit expression

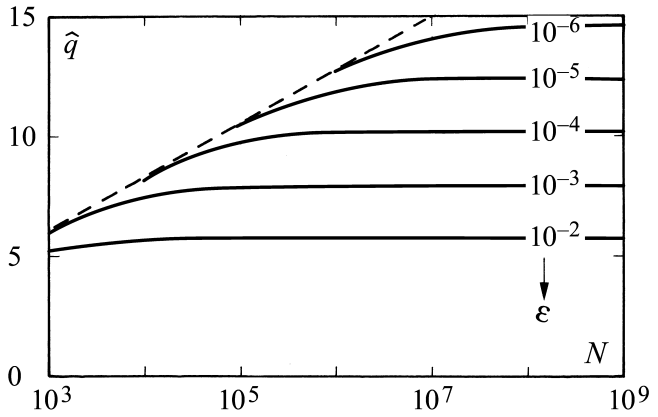

Fig. 2.2 Relative discharge $\hat{q} = Q/(gS_fD^5)^{1/2}$ as function of $N = (gS_fD^3)^{1/2}\nu^{-1}$ for various relative roughnesses $\varepsilon = k_s/D$. (- - -) Smooth flow regime

$$\nu^* = \left[10^{-\sqrt{2}/(\pi D^{*5/2})} - \frac{k_s^*}{3.7D^*}\right]\frac{D^{*3/2}}{1.776}. \tag{2.12}$$

Figure 2.3 shows the smooth flow regime below the envelope curve marked (- - -), while the rough regime is covered by the horizontal lines of the relationship D^* against k_s^*. The plot also shows that D^* varies only between 0.35 and 0.55. An estimated value of $D^* = 0.40$, corresponding to $D = 0.4[Q^2/(gS_f)]^{1/5}$ gives $Q = [gS_f(2.5D)^5]^{1/2}$. The discharge therefore varies with $D^{5/2}$.

The preceding solution procedures involve for all three types of problems an iterative solution with a simple parameter combination. Appropriate values of the *equivalent sand-roughness height* k_s (German: Äquivalente Sandrauhigkeit; French:

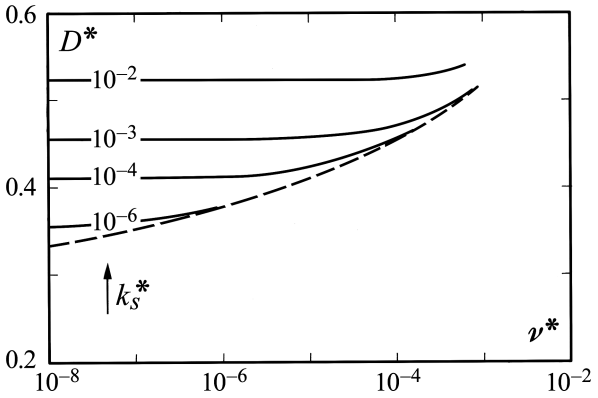

Fig. 2.3 Relative pipe diameter $D^* = D/D_o$ as function of relative kinematic viscosity $\nu^* = \nu D_o/Q$ for various values of $k_s^* = k_s/D_o$ with $D_o = [Q^2/(gS_f)]^{1/5}$. (- - -) Smooth flow regime

Hauteur de rugosité equivalente) in [mm] are presented in Tables 2.1, 2.2 and 2.3. Numerous extraordinary examples of roughness height problems have been reported by Schröder (1990). He also presented methods for roughness determination as well as of the equivalent sand roughness.

Table 2.1 Equivalent sand roughness k_s (excerpted from Richter 1971)

Material and conduit types	Condition	k_s [mm]
drawn and pressed conduit of copper and brass, glass tube	technically smooth, also conduits with metal plating (copper, nickel, chromium)	0.00135–0.00152
plastic pipes	new	0.0015–0.0070
seamless steel pipes rolled and drawn (commercial) new	typical rolled skin	0.02–0.06
	corroded	0.03–0.04
	uncorroded	0.03–0.06
	stainless steel with injection coating of metals	0.08–0.09
	clean zinc coated	0.07–0.10
	commercial zinc coated	0.10–0.16
welded sheet steel, new	typical rolled skin	0.04–0.10
	bitumen coated	0.01–0.05
	cement coated	about 0.18
	galvanized, for pressure charging pipe	about 0.008
used steel pipe	symmetrical rust scars	about 0.15
	moderately rusted, light crusting	0.15–0.40
	moderate crusting	about 0.15
	heavily crusted	2–4
	cleaned after long use	0.15–0.20
	bitumen coated, partly damaged, rusted	about 0.1
	after many years of service	about 0.5
	deposition in sheet form	about 1.1
	25 years in service, irregular tar and naphthalene deposits	about 2.5
cast iron pipes	new, typical cast skin	0.2–0.3
	new, bitumen coated	0.1–0.13
	used, rusted	1–1.5
	crusted	1.5–4
	cleaned after many years of service	0.3–1.5
	city sewers	about 1.2
	heavily rusted	4.5
concrete conduits	new, commercial, smooth tracts	0.3–0.8
	new, commercial, medium rough	1–2

Table 2.1 (continued)

Material and conduit types	Condition	k_s [mm]
	new, commercial, rough	2–3
	new, reinforced concrete, smooth	0.1–0.15
	new, centrifugally cast concrete, smooth	0.1–0.15
	new, centrifugally cast concrete, without plaster	0.2–0.8
	smooth conduit after many years of service	0.2–0.3
	mean value for pipe extension without joints	0.2
	mean value for pipe extension with joints	2.0
asbestos cement pipe	new, smooth	0.03–0.10
earthenware pipe	new, drainage pipe	about 0.7
	new, made from crude clay brick	about 9

Table 2.2 Equivalent sand-roughness height k_s for conduits of various surface characteristics (excerpted from Idel'cik 1979)

Group	Conduit and material type	Condition of surface and type of utilisation	k_s [mm]
I	drawn pipes of		
	brass and copper	technically smooth	0.0015–0.01
	aluminium	technically smooth	0.015–0.06
II	drawn steel pipe without solder joints	new, unused	0.02–0.10
		cleaned after some years of use	up to 0.04
		with bitumen lining	up to 0.04
		hot water pipe	0.20
		oil pipe line, normal	0.20
		medium corrosion with small tar deposits	$\approx$0.40
		water pipe line after long use	1.2–1.5
		with heavy tar deposits	$\approx$3.0
		conduit with poor surface condition	$\geq$5.0
III	welded steel pipe	new or old, in good condition, transition pieces welded or riveted	0.04–0.10
		new, bitumen lined	$\approx$0.05
		long in service, corroded	$\approx$0.10
		long in use, uniform corrosion	$\approx$0.15
		good transition pieces but poor surface condition	0.3–0.4

Table 2.3 Equivalent sand-roughness height k_s (excerpted from ASCE 1969)

Conduit material	Condition	k_s [mm]	$1/n$ [$m^{1/3}s^{-1}$]
CONDUITS			
Asbestos-cement		0.3–3	67–91
brick		1.5–6	58–77
cast iron pipe	new, unlined	0.25	–
	new, bitumen coated	0.12	–
	new, cement coated	0.3–3	67–91
concrete, monolithic	smooth	0.3–1.5	70–83
	rough	1.5–6	58–67
concrete conduit		0.3–3	67–91
corrugated pipe	rough	30–60	38–45
	invert coated	10–30	45–55
	tar lined	0.3–3	67–90
plastic pipe	smooth	3	70–90
burnt clay pipe		0.3–3	70–90
CHANNELS			
lined with			
asphalt		–	60–77
brick		–	55–83
concrete		0.3–0.10	50–90
rip rap		6	30–50
vegetation		–	25–33
excavated			
earth, straight		3	33–50
winding		–	25–40
rock		–	22–33
unmaintained		–	7–20
natural			
small streams		30–1000	–
fairly symmetrical		–	14–30
unsymmetrical, with puddles		–	10–25

2.2.3 *Rough Turbulent Regime*

In the fully developed turbulent flow regime (German: Vollständiges Rauhregime; French: Régime rugueux developpé), the viscous effect is negligible compared to the effect of wall roughness. In this case the friction factor given in Eq. (2.4) simplifies to

$$f = \frac{1}{4}\left[\log\left(\varepsilon/3.7\right)\right]^{-2}, \tag{2.13}$$

and the normalized discharge from Eq. (2.10) is

$$\hat{q} = -\frac{\pi}{\sqrt{2}}\log\left(\varepsilon/3.7\right). \tag{2.14}$$

The corresponding diameter from Eq. (2.12) is

$$k_s^* = 3.7D^* \cdot 10^{-\sqrt{2}}/(\pi D^{*5/2}). \tag{2.15}$$

From these, the following explicit *approximations* were found by Sinniger and Hager (1989)

$$D^* = k_s^{*0.03}/1.853, \quad \text{for} \quad 10^{-8} < \varepsilon < 7.10^4; \tag{2.16}$$

$$D^* = k_s^{*1/16}/1.422, \quad \text{for} \quad 7 \cdot 10^{-4} < \varepsilon < 7 \cdot 10^{-2}. \tag{2.17}$$

Equation (2.17) is of special interest because the range of ε for which it holds coincides with the typical *application range* of ε in hydraulic practice. Its solution for discharge and velocity yields

$$Q = 2.56(gS_f)^{1/2}k_s^{-1/6}D^{8/3}, \quad \text{or} \quad V = 3.256(gS_f)^{1/2}k_s^{-1/6}D^{2/3}. \tag{2.18}$$

The discharge, in this special case, depends strongly on the diameter, rather weakly on the hydraulic gradient S_f and quite insignificantly on the equivalent sand-roughness height k_s.

Historical *flow formulae* (German: Fliessformel; French: Formule d'écoulement) have a form which differ only insignificantly from Eq. (2.18). A comparison of the customary expression $V = (2gS_f)^{1/2}(D/f)^{1/2}$ for the velocity obtained from Eq. (2.3) with Eq. (2.18) yields $f = (1/21.2)(k_s/D)^{1/3}$. Relating the diameter D to the hydraulic radius $R_h = D/4$, and combining with the expression

$$1/n = K = 6.51g^{1/2}k_s^{-1/6} \tag{2.19}$$

where $1/n = K$ [$m^{1/3}s^{-1}$] is a *dimensional roughness factor*, one gets, after Philippe Gauckler (1826–1905), Robert Manning (1826–1897) and Albert Strickler (1887–1963) the well-known GMS relation

$$V = (1/n)S_f^{1/2}R_h^{2/3}. \tag{2.20}$$

In Switzerland one frequently speaks only of the *Strickler formula* (2.20) although it was first proposed by the French scientist Gauckler in 1867. The same Eq. (2.20) was also proposed in 1889 by the Irish Manning on the basis of data measured by Darcy and Bazin and some new experiments carried out by him. In 1895, Manning got this equation modified by another relationship. However, his first formula, Eq. (2.20), although set rather hastily, is still today recognized as the Manning's formula. Albert Strickler, a Swiss engineer, analyzed in 1923 a large number of actual measurements in pressurized pipe and natural stream flows and recommended Eq. (2.20). The merit of his development lies undoubtedly in introducing a formula of the type of Eq. (2.19). Strickler based this on the mean grain diameter of the boundary material of a natural watercourse and found the numerical

value to be 6.72 instead of 6.51 obtained from the preceding consideration. In the following, Eq. (2.20) is designated as the *formula of Manning and Strickler*.

Equation (2.19) allows direct correspondence between K- (or $1/n$) and k_s-values for flows in the fully developed turbulent regime. According to Sinniger and Hager (1989) the following two *application criteria* have to be satisfied:

- Flow in fully developed turbulent regime synonymous with a negligible viscosity effect as

$$k_s > 30\nu(g^2 S_f^2 Q)^{-1/5}; \tag{2.21}$$

- Relative roughness ε in the range

$$7 \times 10^{-4} < \varepsilon < 7 \times 10^{-2}, \tag{2.22}$$

ensuring that neither very smooth nor very rough surfaces are considered.

Even today, 70 years after the proposal of Colebrook and White and nearly 90 years after the basic research of Blasius and Prandtl in Gottingen, the formula of Manning and Strickler still is relevant. This is particularly established by two facts:

- First, as shown below, the difficulty in the determination of a lumped $1/n$-value for the boundary surface does not allow an "exact calculation" of discharge, and
- Second, a simple exponential formula offers advantages for the practical calculation of typical parameters such as the discharge Q, the velocity V or the diameter D, particularly for free surface flow.

Basically, a *minimum value* of $1/n = 20\ \mathrm{m^{1/3}s^{-1}}$ satisfies the application criteria of Eqs. (2.21) and (2.22). The *maximum value* is $1/n = 90\ \mathrm{m^{1/3}s^{-1}}$, and the minimum friction slope is $S_f = 0.1\%$. Further, it is repeated that Eq. (2.4) or also Eq. (2.10) are strictly valid only for prismatic conduits with uniform distribution of surface roughness. Table 2.4 gives the numerical values for the roughness factor. From this, a distinction in the status of the wall condition as good, normal and bad may be observed. Table 2.4 does not indicate the temporal development of the $1/n$-values, that is, their change with age.

Tables 2.4 and 2.5 specify the accuracy of the flow formula. According to Eq. (2.20) the velocity and consequently the discharge are directly proportional to the $1/n$-value. Usually, a $1/n$-value is given within $\pm 5\%$ accuracy for surfaces of known manufacture. For old channels, deviations in the estimation of $1/n$ of at least $\pm 10\%$ occur provided no detailed measurements are available. The *accuracy of the flow formulae* is therefore related to the difficulty in the estimation of the $1/n$-value. Despite these practical shortcomings, the determination of an exact $1/n$-value shall follow the computation for conduits with the most exact disposal of the relations.

Table 2.4 Friction coefficient $1/n$ [$m^{1/3}s^{-1}$] for formula of Manning and Strickler in relation to boundary condition (excerpted from Chow 1959)

	Wall condition		
Type of wall	good	medium	poor
cast iron, uncoated	85	70	65
cast iron, coated	90	85	75
steel	75	65	60
earthware	90	75	65
clay (drainage pipe)	85	70	60
concrete	85	65	60
polished brick	90	75	65
brick masonry	85	65	60
finished concrete	90	85	75
with concrete coating	85	65	55
broken stone in mortar	60	50	35
dry stone rubble	40	30	25
masonry work	75	65	60

Table 2.5 Friction factor $1/n$ [$m^{1/3}s^{-1}$] for formula of Manning and Strickler as function of wall condition (excerpted from Naudascher 1987)

Channel description	$1/n$ [$m^{1/3}s^{-1}$]
SHEET METAL DUCTS	
smooth conduits with countersunk rivet heads	90–95
new cast iron conduits	90
riveted conduits, rivets not countersunk	65–70
CONCRETE CHANNELS	
with smooth cement finish	100
with steel shuttering	90–100
with smooth plaster	90–95
with smoothened concrete	90
with smooth undamaged cement plaster	80–90
using timber shuttering, without plaster	65–70
rammed concrete with smooth surface	60–65
old concrete, clean faces	60
coarse concrete lining	55
unsymmetrical concrete faces	50
MASONRY CHANNELS	
made of brick masonry work, also clinker, well jointed	80
made of dressed stone	70–80
made of carefully laid broken stone masonry work	70
made of masonry work (normal)	60
crudely made broken stone masonry work	50
made of broken stone walls, slopes plastered	45–50

Table 2.5 (continued)

Channel description	$1/n$ [$m^{1/3}s^{-1}$]
EARTHEN CHANNELS	
In rigid material, smooth	60
In non-mobile sand with some soil and gravel	50
with bed of sand and gravel, plastered sides	45–50
In fine gravel, about 10/20/30 mm	45
In medium gravel, about 20/40/60 mm	40
In coarse sized gravel, about 50/100/150 mm	35
In loamy soil	30
laid with coarse stone aggregate	25–30
In sand, clay or gravel, heavy growth	20–25
NATURAL WATERCOURSES	
with rigid bed, regular	40
with moderate rubble	33–35
with vegetal cover	30–35
with rubble, irregular	30
with strong sediment transport	28
with coarse rubble, about 0.2–0.3 m	25–28
with coarse rubble, with sediment transport	19–22

The Manning and Strickler formula is normally sufficient for fully-developed turbulent flow, whereas Eqs. (2.21) and (2.22) have to be checked for larger structures, and the generalized formula of Colebrook and White has to be applied otherwise.

As is yet to be shown, the formulae of Colebrook and White and of Manning and Strickler can be generalized simply for flows in *free-surface channels*. Therefore, the surface characteristics of such conveyance systems are also represented in Tables 2.1 and 2.2. A particular generalization of the Manning and Strickler formula is presented in Chap. 3.

2.3 Local Losses

2.3.1 *Description*

Local losses occur wherever the streamlines are directed away from the axial direction of flow due to either a change in the wall geometry, or lateral discharge addition or reduction. The main flow then either accelerates or is retarded. Specially for decelerated flow, particles close to the boundary cannot follow the average velocity of the one-dimensional streamtube and separate laterally from the main flow. In the regions of large direction change – as the example in Fig. 2.4 shows – both primary and secondary flow regions exist. For a *diffusor*, essentially an enlargement of the cross-section (Fig. 2.4a), the main current does not follow the walls and two marked zones of *separated flow* appear on the two sides of the main stream in the widened downstream part of the diffusor, where the main stream has not yet fully expanded.

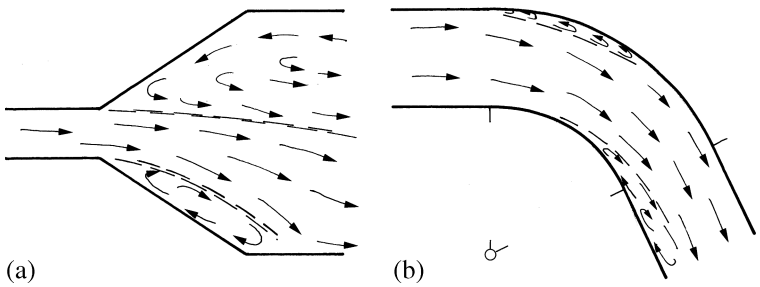

Fig. 2.4 Local losses (**a**) diffuser flow, (**b**) bend flow. Schematic subdivision into primary and secondary flow zones, with (- - -) shear boundary

The separated flows extract considerable energy from the main stream, contributing thereby substantially to the local losses.

In *bend flow* shown in Fig. 2.4b, complicated phenomena can appear as for diffusor flow. Owing to the high pressure at the outer bend side, the particles at the interface do not follow the primary stream but are drawn laterally into the secondary flow zone. Further downstream, there exists an analogue situation along the inner bend wall contributing essentially to the bend losses. These are caused mostly by flow separation and not due to the reattachment of the separated flow (Eck 1991).

Hydraulic separation zones are characterized by high turbulence phenomena, i.e. all flow parameters have a marked dynamic flow component. According to Reynolds, any one of these parameters, e.g., the local pressure intensity p, can be represented as the sum of a *temporal mean value* $\bar{p}$ and a *turbulent fluctuation component* p'. Consequently, for steady discharge, the integrated fluctuating component $\int p' \mathrm{d}t$ over a sufficient time period must equal zero. The turbulence number T represents the ratio of a convenient value of the fluctuating component p' (such as the standard deviation) and the temporal mean value $\bar{p}$ corresponding, for example, to $(\overline{p'^2})^{1/2}/\bar{p}$ ensuring a positive number. The turbulence number remains small in the main flow region; in the zone of secondary flow, however, it increases to large orders of magnitude. The maximum value, relative to either pressure or velocity, appears normally at the shear layer as also along the fluctuating boundary line or boundary surface between the primary and the secondary flows (Fig. 2.4). The complex phenomena inside a separation zone are frequently of little interest; more important from the practical standpoint is the answer to the question: How can the flow losses be reduced? The answer requires fundamental knowledge of the flow mechanisms so that different kinds of elements can be compared with each other. This requires defining the so-called dimensionless loss coefficients or resistance values (Eck 1991).

For turbulent flows occurring in practice, the viscous losses are often insignificant. The local losses are then strongly dependent on the velocity field only. Based on Bernoulli's equation (1.15) the energy head H is represented as the sum of the static and the dynamic pressure heads $H = (p_s + p_d)/(\rho g)$, where p_s and p_d are measured, respectively, perpendicular and tangential to the streamline direction.

As *dynamic pressure* one therefore designates the expression $p_d/(\rho g) = V^2/(2g)$. The total (subscript g) pressure is equal to the sum $p_g = p_s + p_d$.

The local energy loss ΔH_L is closely linked with the dynamic pressure p_d. If the fluid is not in motion ($p_d = 0$), no losses are expected. As the velocity of the fluid increases, larger losses occur. The preceding discussion indeed shows that the local losses are proportional to the dynamic pressure, resulting in an almost constant number for the ratio of energy loss and dynamic pressure head. This number is referred to as the *loss coefficient* (German: Verlustbeiwert; French: Coefficient de perte de charge)

$$\xi = \Delta H_L/(V_i^2/2g), \tag{2.23}$$

where V_i is a well defined reference velocity. In practice, it is often stated that:

- Either the quantity V_i is poorly or not at all defined, or
- Calculations are carried out using incorrect reference velocities.

It is therefore important to correctly define ξ-values as well as the *reference velocity* V_i. In particular, all basic quantities are to be so selected that no problems arise for their determination. Frequently, V_i is set equal to the nominal velocity, for example, the mean value of the incoming or the outgoing velocities in the flow elements being investigated. Usually reference to the larger of the two values is made, e.g. the approach flow velocity for the case of Fig. 2.4a. For combining flow, V_i is usually taken as the downstream velocity whereas, for flow division, one refers to the cross-section of the approach flow. Consequently, the reference velocity remains always positive and larger than zero.

Further characteristics of the loss coefficients are explained with examples by Naudascher (1987). A close connection between the loss coefficient ξ and the resistance coefficient c_w is indicated. Flows around *bridge piers* and *trash rack* structures are explained by:

- Reynolds number and pier or bar shapes,
- Roughness and turbulence effects,
- Bottom and ends of piers,
- Wave build up and resulting structural vibration, and
- Constrictions and arrangement of adjacent structures.

In these cases, extensive experimental material exists which is not always available for other structures. For practical purposes this abundance of data is not always available, and reference to *guidance values* of ξ is made. For further information, one should consult the standard works of Richter (1971), Miller (1971, 1978), Idel'cik (1979, 1986), Ward-Smith (1980), and Blevins (1984). The abundance of data material contained in these sources cannot be discussed here.

In the following, a selection of values for the loss coefficient ξ is presented, refering to standard cases and valid, basically, only for *pressurized flow*. The transformation of these results to free surface flow is discussed in 2.4. The flow elements considered are bends, contractions, expansions, inlets and outlets, combining and dividing junctions and special sewer elements. For the cross-sectional form of these elements, mainly the *circular profile* is considered.

2.3.2 *Conduit Bend*

The wall pressure along a *circular bend* (German: Kreiskrümmer; French: Coude circulaire) changes as shown in Fig. 2.5. On both sides of the element the pressure line has a gradient S_f, which steepens along the bend and merges with the gradient S_f further downstream.

The computation of the *energy loss* ΔH_L along the bend is simplified by assuming that the distributed losses are locally concentrated and measured as the vertical distance between the undisturbed energy lines. For an experimental investigation, first the bend is not considered and the equivalent sand roughness height of the conduit material is ascertained. Then, the bend is accounted for, and the value of ΔH_L is separately determined. For the computational determination of ΔH_g, the procedure is reversed. Regarding the friction loss, the presence of the bend is first neglected, the term ΔH_R calculated along the conduit and at the end, the local loss is added with Eq. (2.1). This procedure therefore considers that the loss producing element involves no length. Also, the substantial loss occurs not along the bend but manifests itself in the *downstream reach*, as is clear from Figs. 2.4b and 2.5.

The loss coefficient ξ_k for the circular bend (subscript k) depends essentially on the ratio of the bend mid-radius R and the pipe diameter D, the angle of deviation δ and the Reynolds number $\mathsf{R} = VD/\nu$. Figure 2.6a shows experimental curves after Ito

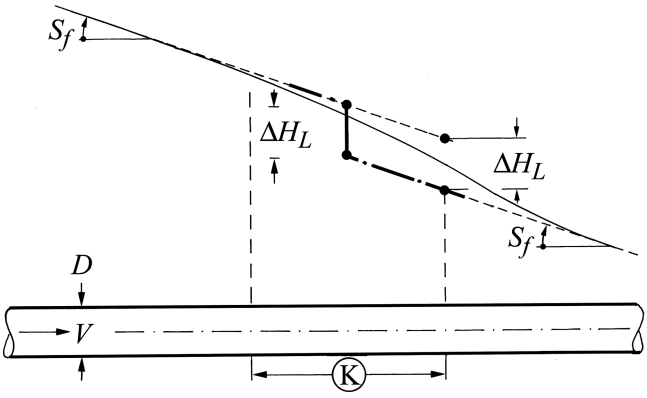

Fig. 2.5 (—) *Pressure line* along a *circular bend* K, (- - -) gradient S_f, (···) computational curve with locally concentrated bend loss ΔH_L

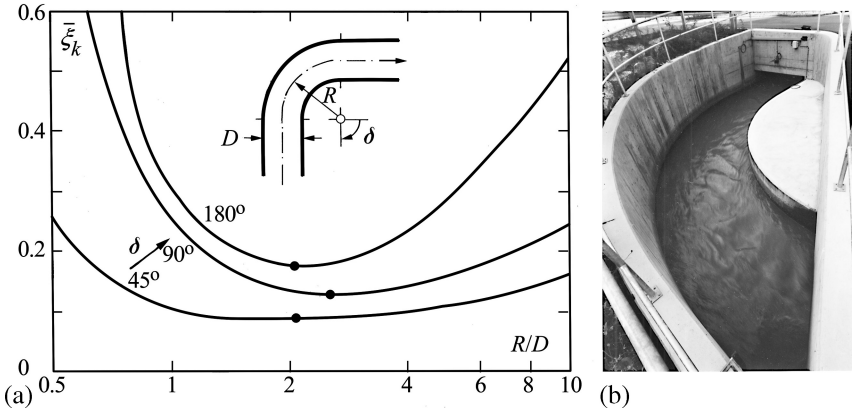

Fig. 2.6 (**a**) Total loss coefficient $\bar{\xi}_k = \Delta H_k/(V^2/2g)$ as a function of relative bend radius R/D and angles of curvature δ for $\mathsf{R} \geq 10^6$ after Ito (1960) and Blevins (1984), (•) minimum value, (**b**) Typical open channel bend structure on treatment station

(1960), for a Reynolds number $\mathsf{R} = 10^6$ corresponding to a velocity around 1 ms^{-1} for a typical pipe diameter of 1 m. This study includes the influence of the friction loss along the curve. It is evident from Fig. 2.6a that for every angle δ there exists a *minimum value* (subscript m) of the total loss coefficient ξ_{km} for R/D of about 2. This behaviour reflects the fact that:

- For small bend radius R/D, the separation zone is large, and
- For large bend radius R/D, the influence of friction is dominant.

Between these two extremes lies the optimum value of R/D between 2 and 3. The curves represented in Fig. 2.6a are minimum values. If the Reynolds number R is smaller than 10^6, the value ξ_k obtained from Fig. 2.6 are multiplied by $(10^6/\mathsf{R})^{1/6} > 1$.

Figure 2.7 represents the appropriate *loss coefficient* ξ_k after Miller (1971). There appears likewise an optimum curvature R/D between 1 and 3 in this figure. For $R/D = 2$ the loss coefficient ξ_k does not exceed 0.2 even for 180°. For practical purposes the mid-radius R of the bend should be chosen to be about *double* the pipe diameter. On the other hand, the representation also points to the result that ξ_k values increase steeply for deviations greater than 60°. Therefore, an angle of 90° should be considered the upper limit of a hydraulically well designed conduit.

Figure 2.7 was derived for a Reynolds number $\mathsf{R} = VD/\nu \cong 10^6 (\log \mathsf{R} = 6)$. For a different Reynolds number R, the correction to be applied is (Sinniger and Hager 1989)

$$\xi_k/\xi_k(\mathsf{R} = 10^6) = \frac{3.7}{\log \mathsf{R} - 2.3}. \tag{2.24}$$

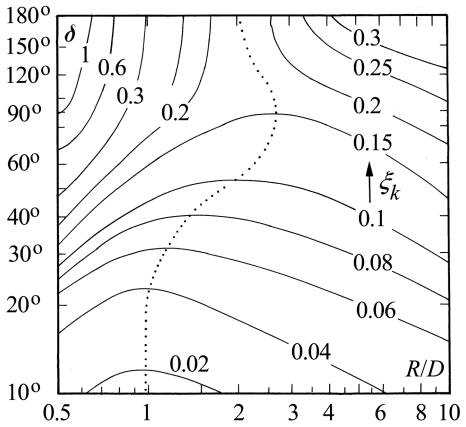

Fig. 2.7 Loss coefficient ξ_k for conduit bend after Miller (1971) as function of relative radius of curvative *R*/*D* and angle of deviation δ for circular cross-section and $\mathsf{R} = 10^6$, (...) minimum value

Double bends consisting of two 90°-degree bend elements lying a distant L_k apart were considered by Blevins (1984). The ratio Ξ of the total ξ_k-value to the sum (subscript tot) of the individual values $\xi_{k\text{tot}}$ varies with the relative curvature *R*/*D* and with the relative distance L_k/D, where L_k is measured from the end of the first to the beginning of the second bend. For $L_k/D > 20$, $\Xi = 1$, for smaller relative distance $\Xi < 1$, however, such as $\Xi = 0.85$ for $L_k/D = 0$. With the usual assumption $\Xi = 1$, the resulting loss is overestimated. The values of the coefficient for two 90°-degree bends located at two different levels are given similarly. There appears to be practically no difference with the levels of installation of the double bend. Table 2.6 gives the detailed results.

Mitre-bends (German: Kniekrümmer; French: Coude abrupt) in which the change of direction is abrupt, are not generally recommended for sewers. For direction changes as small as $\delta = 40°$, the loss coefficient is already as high as $\xi_k = 0.25$, and for $\delta = 90°$, ξ_k is about 1.2, much larger than the minimum loss coefficient for

Table 2.6 Loss coefficient $\Xi = \xi_{k\text{tot}}/\Sigma\xi_{ki}$ for two 90°-bends in tandem arrangement (**a**) in one plane, (**b**) in two planes

		L_k/D				
	R/*D*	0	4	10	20	30
(a)	1.85	0.86	0.72	0.82	0.95	0.96
	3.3	0.84	0.82	0.86	0.96	1.0
	7.5	0.93	0.96	0.97	1.0	1.0
(b)	1.85	0.88	0.73	0.86	0.96	0.97
	3.3	0.86	0.81	0.88	0.97	1.0

circular bends. A series of detailed information on mitre bends have been presented by Sinniger and Hager (1989) and Hager (1992).

2.3.3 *Expansion*

The degree of an expansion (German: Erweiterung; French: Expansion) is usually described with the angle of expansion δ and the cross-sectional area ratio F_1/F_2 of the expansion (subscript e). The *loss coefficient* $\xi_e = \Delta H_{12}/(V_1^2/2g)$ involves the approach flow velocity V_1 (Fig. 2.8).

Conduit expansions are characterized by asymmetrical flow behaviour. For the diameter ratio $D_2/D_1 > 1.4$, the jet entering the expansion attaches to one of its two downstream walls (Fig. 2.8a) and, depending on the expansion angle, the Reynolds number and the expansion ratio, the jet becomes either oscillating or stably asymmetric. The velocity ratios, the wake structure and the resulting consequences for *diffusors* are summarized by Blevins (1984) and Hager (1990). These are not pursued further here.

With regard to expansion losses, the *abrupt* 90°-*diffusor* has special significance because the loss coefficient may be determined from elementary hydraulic considerations. Assuming that the pressure acting on the expansion face is the same

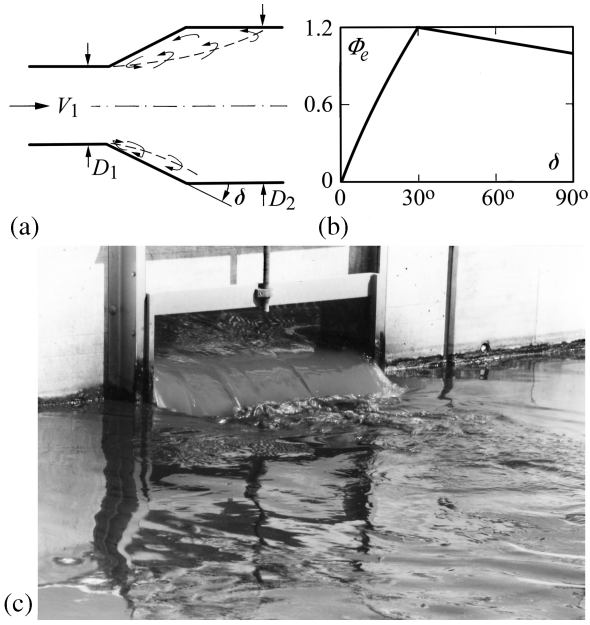

Fig. 2.8 Conduit expansion (**a**) definition plot and flow structure, (**b**) loss coefficient $\Phi_e = \Delta H_{12}/(V_1^2/2g)$ as function of the expansion angle δ. (**c**) Expanding jet from an outlet into an aeration basin

as the inlet pressure p_1 and neglecting the wall resistance, the application of the momentum principle yields the Borda-Carnot expression

$$\xi_{e90^\circ} = \Delta H_{12}/(V_1^2/2g) = [1 - (F_1/F_2)]^2. \tag{2.25}$$

ξ_{e90° is defined with respect to the approach flow velocity V_1. For circular conduit diffusors, the loss coefficient depends on the ratio of diameters (D_1/D_2) only.

In analogy to this special case, the effect of the *expansion angle* δ on ξ_e is accounted for with the relation

$$\xi_e = \Phi_e(\delta) \cdot \xi_{e90^\circ}. \tag{2.26}$$

Equation (2.26) splits the loss coefficient ξ_e in two parts, one depending only on the angle δ and the other depending only on the area ratio F_1/F_2. The experimentally measured values of $\Phi_e(\delta)$ can be represented as (Sinniger and Hager 1989)

$$\Phi_e(\delta) = \frac{\delta}{90^\circ} + \sin(2\delta), \qquad 0 \le \delta \le 30^\circ; \tag{2.27}$$

$$\Phi_e(\delta) = \frac{5}{4} - \frac{\delta}{360^\circ}, \qquad 30^\circ \le \delta \le 90^\circ. \tag{2.28}$$

These two relations satisfy the limit conditions $\Phi_e(\delta = 0) = 0$ and $\Phi_e(\delta = 90^\circ) = 1$ (Fig. 2.8b). The maximum value occurs around $\delta = 30^\circ$. Tests indicate that expansions behave hydraulically similar for δ greater than about 30°. Low values for the losses occur only for small expansion angles ($\delta < 10^\circ$). The maximum ξ_e value is somewhat larger than 1, and the entire approach velocity head is dissipated.

A *conduit outlet* (German: Rohrauslauf; French: Exutoire de conduite) can be considered a special case of an expansion. For example, if an *outfall conduit* discharges into a basin or into the sea, the expansion ratio tends to $F_1/F_2 \to 0$. Eq. (2.25) then gives $\xi_{e90^\circ} = 1$ and the loss coefficient follows $\xi_e = \Phi_e(\delta)$. For $\delta > 30^\circ$ and expansions with a large downstream section, all kinetic energy is dissipated.

The relationships derived previously apply only for an outfall conduit discharging under water. For an outflow conduit discharging into *air* as a compact jet, there is practically no loss. Further information on conduit expansions together with a comprehensive literature review is presented by Sinniger and Hager (1989).

2.3.4 *Contraction*

Although the contraction geometry equals a reversal of flow direction in a conduit expansion, the flows in the two elements are expected to be fundamentally different,

owing to the differences in the separation structures. As schematically represented in (Fig. 2.9a), the flow in a sharp-edged contraction (German: Verengung; French: Contraction) experiences an additional contraction K and expands downstream to the full cross-sectional area F_2. As is well known, a contracted flow is nearly free of energy loss and the loss in the contraction element must be attributed to the *expansion of flow* downstream of the contracted flow. Contraction (subscript v) flow is essentially influenced by the angle of contraction δ and the area ratio $\phi = F_2/F_1 < 1$.

Few experimental studies exist for conduit contractions. Of particular relevance is a paper by Gardel (1962). The relationship derived for the loss coefficient ξ_v is

$$\xi_v = \Delta H_{12}/(V_2^2/2g) = \frac{1}{2}(1-\phi)(\delta/90°)^{1.83(1-\phi)^{0.4}}. \tag{2.29}$$

It is noted that the contraction loss coefficient is always smaller than the corresponding expansion loss coefficient. Also, ξ_v increases substantially with the contraction angle δ; and Eq. (2.29) yields moderate losses for contraction angles below $\delta < 30°$. For $\delta = 90°$, $\xi_v = (1-\phi)/2$, i.e., the loss increases linearly with the decrease in the contraction ratio. Additional information on this topic has been reported by Benedict et al. (1966).

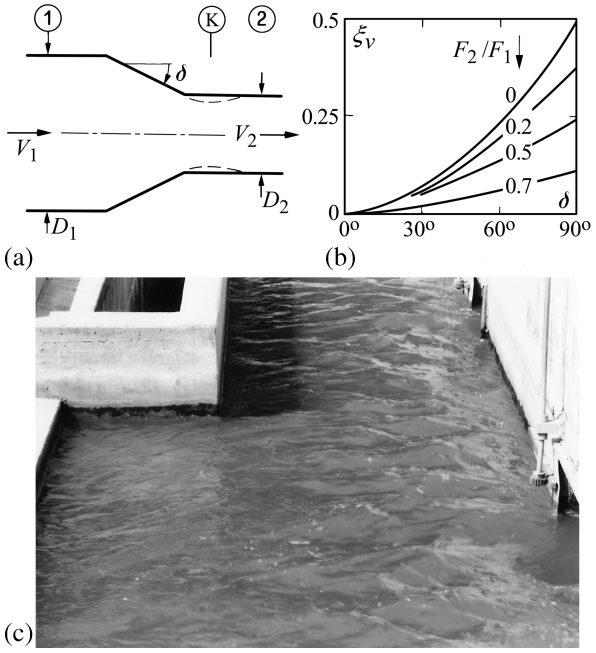

Fig. 2.9 Conduit contraction (**a**) definition and flow structure, (**b**) loss coefficient $\xi_v = \Delta H_{12}/(V_2^2/2g)$ as function of contraction angle δ for various values of area ratio $\phi = F_2/F_1$ after Gardel (1962). (**c**) Contracting main channel due to laterals in a distribution channel

A *conduit inlet* (German: Rohreinlauf; French: Pertuis d'entrée) can be treated as a special case of a contraction element with the area ratio tending to zero. It follows from Eq. (2.29) that $\xi_v(\phi = 0) = (1/2)(\delta/90°)^{1.83}$; for the usual case $\delta = 90°$, the loss coefficient is thus $\delta_v = 0.5$. For a sharp-edged conduit inlet, therefore, the head loss is half the pipe velocity head $(1/2)\,[V_2^2/(2g)]$. This high value of the conduit velocity head may be reduced by *rounding* (German: Ausrundung; French: Courbure) the contraction inlet with the radius r_v. The data by Idel'cik (1979) can be approximated as

$$\xi_v = \frac{1}{2}\exp(-15 r_v/D). \tag{2.30}$$

Figure 2.10b shows that the loss coefficient decreases sharply with the relative rounding radius. Comparing Eq. (2.30) with the work of Knapp (1960) one observes for $r_v/D > 1/6$ practically no inlet loss. Similarly, not much pressure difference exists in this case between the conduit axis and the boundary wall streamline. The rounding of sharp edges has a strong hydraulic effect but the *point of separation* is no longer clearly defined. Rounded transition elements may further be quite expensive.

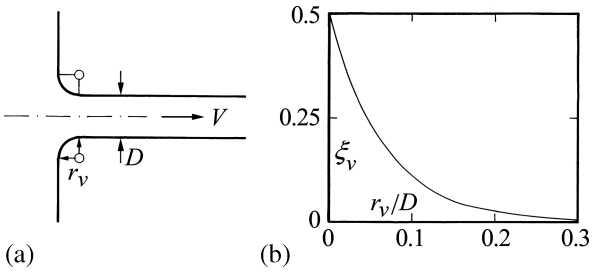

Fig. 2.10 Rounded conduit inlet (**a**) definition sketch, (**b**) loss coefficient $\xi_v = \Delta H_v/(V^2/2g)$ as function of the relative rounding radius r_v/D

2.3.5 *Combining Conduit Junction*

In conduit systems, combining and dividing conduits are frequently encountered (see also 2.3.6). The corresponding loss coefficients may be quite high and it is important to consider their numerical magnitudes, therefore.

Figure 2.11a shows a definition sketch for the combining conduit (German: Rohrvereinigung; French: Combinaison de conduites). In principle, the flow continuing from the upstream branch (subscript o) is distinguished from the lateral branch (subscript z) that enters the flow system. The combining angles are referred to as δ_o and δ_z, and the cross-sectional areas are F_o and F_z, respectively. The discharge

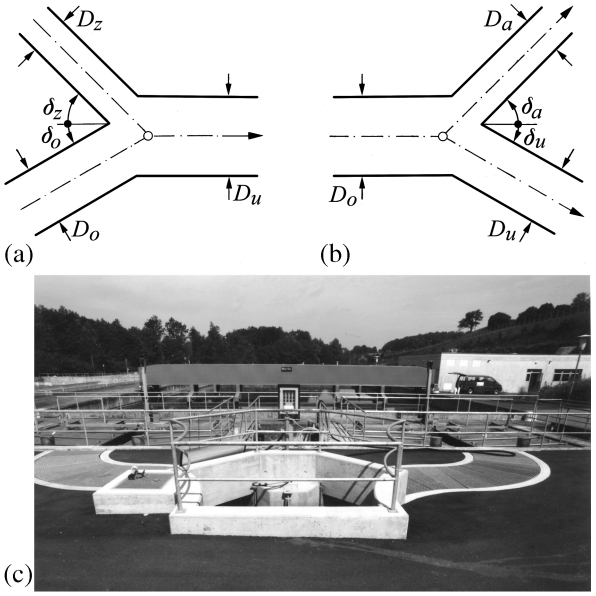

Fig. 2.11 Schematic representation and notation for (**a**) combining conduit, (**b**) dividing conduit. (**c**) Junction structure on treatment station

ratio remains always between zero and unity and the outflow is designated Q_u. The relative inflow is, consequently, $q = Q_z/Q_u$ such that $Q_o = Q_u – Q_z = Q_u(1–q)$. For the area ratios, one considers likewise the downstream cross-sectional area F_u as the reference quantity which gives

$$m = F_z/F_u, \quad n = F_o/F_u, \quad q = Q_z/Q_u. \tag{2.31}$$

The *loss coefficients* for the lateral and the upstream branches, respectively, are defined as

$$\xi_z = \frac{H_z - H_u}{V_u^2/2g}, \quad \xi_o = \frac{H_o - H_u}{V_u^2/2g}. \tag{2.32}$$

Both values are non-dimensionalized with respect to the downstream velocity $V_u > 0$.

Combining flows are analyzed using the basic principles of pressure distribution together with the momentum equation. Vischer (1958) obtained the loss coefficients for the conduit junction involving *sharp edges* as

$$\xi_z = 1 - 2m^{-1}\, q^2\, \cos\delta_z - 2n^{-1}(1-q)^2\, \cos\delta_o + (m^{-1}q)^2, \tag{2.33}$$

$$\xi_o = 1 - 2m^{-1}\, q^2\, \cos\delta_z - 2n^{-1}(1-q)^2\, \cos\delta_o + [n^{-1}(1-q)]^2. \qquad (2.34)$$

These two relations differ only in their last terms. The loss coefficients depend on five independent parameters δ_o, δ_z, m, n and q. *Special cases* result for $n = 1$ ($F_o = F_u$) and $\delta_o = 0$ (upstream and downstream branches connected with a straight line). Then, the results of Favre (1937) apply

$$\xi_z = -1 + 4q + (m^{-2} - 2m^{-1}\, \cos\delta_z - 2)q^2, \qquad (2.35)$$

$$\xi_o = q[2 - (1 + 2m^{-1}\, \cos\delta_z)q]. \qquad (2.36)$$

These relationships are also developed by Idel'cik (1986). The evaluation of Eqs. (2.33) and (2.34) shows that the influence of the junction angle δ_z on both ξ_z and ξ_o is small. Figure 2.12 shows the representation for $\delta_z = 45°$, which changes only slightly for other angles δ_z. The figure also shows the large influence of both the remaining parameters m and n on ξ_o and ξ_z. With the exception of small values of q, ξ_z is always positive and the energy head of the lateral inflow is always larger than the downstream energy head H_u for large values of the lateral inflow. In contrast, for all large values of q, ξ_o is negative, i.e. the water from the upstream branch is sucked in by the incoming lateral flow, similar to a water jet pump. For the upstream branch, therefore, the mechanical energy increases, resulting in a *negative* value for the loss coefficient ξ_o. The total energy budget corresponding to the sum of energies in the upstream and lateral branches is naturally always larger than the energy in the downstream branch.

Of practical interest are the conduit junctions of minimum energy loss. Apart from the case with $\delta_o \to 0$ and $\delta_z \to 0$ in which both the incoming flows enter the main stream with minimum possible lateral component, the expressions for the *optimum area ratios* (subscript opt) are (Vischer 1958)

$$m_{\text{opt}} = q/\cos\delta_z, \quad n_{\text{opt}} = (1-q)/\cos\delta_o. \qquad (2.37)$$

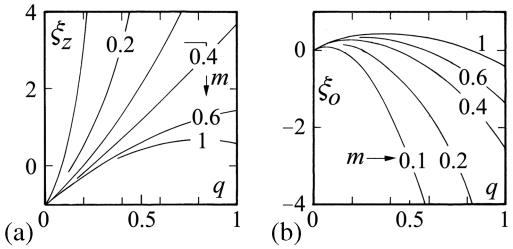

Fig. 2.12 Loss coefficient in combining conduit junction for $\delta_z = 45°$ and $\delta_o = 0$ for (**a**) lateral branch ξ_z and (**b**) upstream branch ξ_o in relation to discharge ratio $q = Q_z/Q_u$ for various area ratios $m = F_z/F_u$ and $n = 1$

These relations express that the projections of the cross-sectional areas F_o and F_z on the downstream conduit correspond to the respective quantity distribution in the two branches of inflow. For variable discharge ratio q, the optimum values are retained for the design discharges.

Small values for the loss coefficients result for comparable velocities in the three branches and sharp edges in the junction element are eliminated by appropriate *rounding*. Further results can be derived from the extensive measurements reported by Gardel (1957) as well as by Gardel and Rechsteiner (1970). Ito and Imai (1973) summarized these studies and presented empirical equations. The rounded conduit junctions are treated in Sect. 16.2.2.

2.3.6 *Dividing Conduit Junction*

Whereas the combining flow in a conduit junction has a flow structure similar to that in a conduit contraction (and thereby remaining amenable to elementary calculations), a conduit junction for flow division (German: Abflusstrennung; French: Séparation d'écoulement) is analogous to a conduit expansion. Losses in both elements are governed by *flow separation* from the walls, a phenomenon that becomes more pronounced with decreasing velocity.

Designating the flow from the upstream branch with subscript o, the lateral flow branch with subscript a and the downstream flow branch with subscript d (throughflow), the loss coefficients for flow division (Fig. 2.11b) are defined analogous to those for the combining flow as

$$\xi_a = \frac{H_o - H_a}{V_o^2/2g}, \quad \xi_d = \frac{H_o - H_d}{V_o^2/2g}. \tag{2.38}$$

The loss coefficients are defined with reference to the non-zero inflow velocity V_o. Assuming a plausible distribution of the lateral division angle δ_a, Hager (1984) calculated for $F_o = F_a = F_d$ and $\delta_d = 0$ with $\bar{q}=Q_a/Q_o$

$$\xi_a = 1 - 2\bar{q}\cos\left(\frac{3}{4}\delta_a\right) + \bar{q}^2, \tag{2.39}$$

$$\xi_d = \frac{4}{5}\bar{q}\left(\bar{q} - \frac{1}{2}\right). \tag{2.40}$$

Idel'cik (1979) studied configurations with $\delta_d = 0$ and F_a+$F_d = F_o$, i.e. equal cross-sectional areas of the approach and downstream branches. Denoting the velocity ratios

$$\mu_a = V_a/V_o, \quad \mu_d = V_d/V_o, \tag{2.41}$$

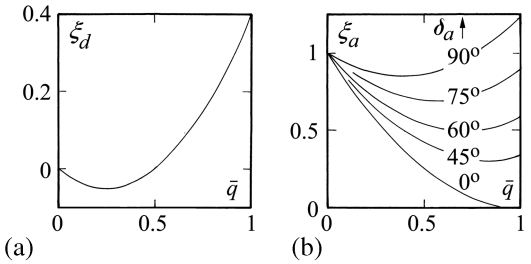

Fig. 2.13 Loss coefficients for conduit division with $F_o = F_a = F_d$, (**a**) through branch and (**b**) lateral branch as functions of the through discharge ratio $\bar{q} = Q_a/Q_o$ and lateral division angle δ_a

one obtains approximately

$$\xi_a = 1 - 2\,\mu_a \cos\delta_a + (1 - \sin^3\delta_a)\mu_a^2, \tag{2.42}$$

$$\xi_d = (1 + \mu_d)(1 - \mu_d)^2. \tag{2.43}$$

In general, the loss coefficient ξ_d for the through branch is *independent* of the off-take angle δ_a. Further, for small relative lateral discharge $\bar{q} << 1$, the value of ξ_a is nearly unity. Therefore, if almost the entire fluid flows downstream, the velocity head of the upstream branch is dissipated. The effect of rounding the sharp edges is substantial and has been investigated by Idel'cik (1986).

2.3.7 *Y-Junction*

By the term Y-junction one understands a symmetric conduit junction for either combining or dividing flow, as shown in Fig. 2.14. In a *T-junction*, the two approach branches are perpendicular to the downstream branch, or the two downstream branches are perpendicular to the approach flow branch. The following considers the cases $\delta_z = \delta_o$ for combining flow, and $\delta_a = \delta_d$ for flow division. First, three branches of equal cross-sectional area are considered, and second the total inflow and total outflow cross-sectional areas are assumed equal. The relevant information originates from Miller (1978).

For *combining flow* in T-junctions (subscript T) the results of Idel'cik (1979) are considered. The loss coefficient $\xi_{Tv} = \Delta H_{Tv}/(V_u^2/2g)$ is expressed in terms of the velocity head of the downstream branch, $q_z = Q_z/Q_u$ is the discharge ratio and $\phi = F_u/F_z$ the ratio of the cross-sectional areas of the downstream to the lateral branches. Then, for $\delta_z = 90°$,

$$\xi_{Tv} = 1 + \phi^2 + 3\phi^2(q_z^2 - q_z). \tag{2.44}$$

The ξ_{Tv} curves are symmetrical with respect to the optimal ratio $q_z = 0.5$ and the loss coefficient is always larger than unity (Fig. 2.15a). The loss coefficient is considerably reduced by inserting a *division wall* (Fig. 2.15b) and then amounts to

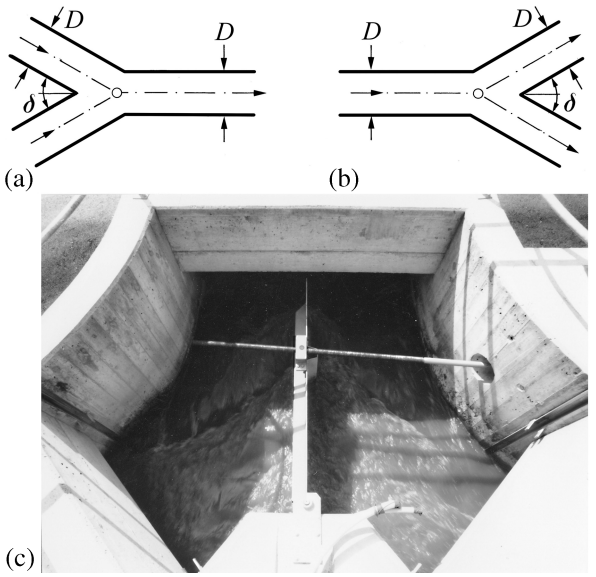

Fig. 2.14 Y-junction for (**a**) combining flow and (**b**) flow division. (**c**) Typical junction structure on wastewater treatment station

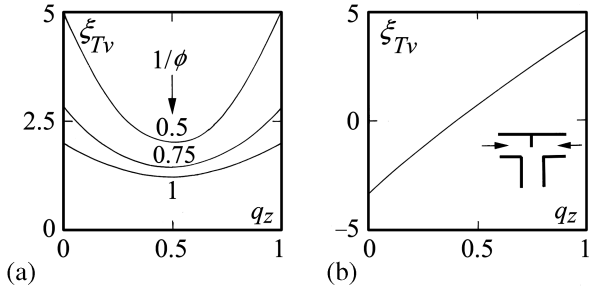

Fig. 2.15 Loss coefficient of combining flow in T-junction, $\xi_{Tv} = \Delta H/(V_u^2/(2g))$ as a function of discharge ratio $q_z = Q_z/Q_u$ and the area ratio $1/\phi = F_z/F_u$ for $\delta_z = 90°$, (**a**) without division wall, (**b**) *with* division wall

$$\xi_{Tv} = 7(q_z - 0.4). \tag{2.45}$$

The loss coefficients for the other branches are determined with the corresponding discharge ratios.

The *flow division* in a Y-junction was studied by Miller (1978). Figure 2.16 shows the experimental results for all three branches of equal cross-sectional area as also with equal cross-sectional areas for the upstream and downstream branches. In order to keep the losses within reasonable limits, one should limit the dividing angle to less than 60° and use symmetrical flow conditions.

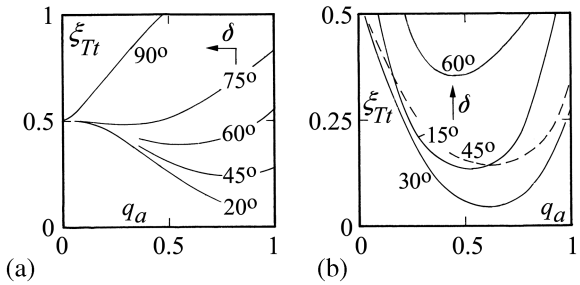

Fig. 2.16 Flow division in Y-junction, $\xi_{Tt} = \Delta H_{Tt}/(V^2/2g)$ as function of discharge ratio $q_a = Q_a/Q_o$ for various division angles δ (Miller 1978). (**a**) identical cross-sectional area, (**b**) equal cross-sectional area of up- and downstream branches

2.3.8 *Trash Racks*

Figure 2.17a shows a trash rack (German: Einlaufrechen; French: Grille d'entrée) set in an open channel at an angle δ_{Re} relative to the direction of flow. The approach flow velocity is V_o and the rack (subscript *Re*) loss is ΔH_{Re}. The loss coefficient expressed in terms of the approach flow velocity V_o is (Sinniger and Hager 1989)

$$\xi_{Re} = \beta_{Re}\, \zeta_{Re} c_{Re} \sin\delta_{Re} \tag{2.46}$$

with β_{Re} as the rack coefficient (Table 2.7) shown in Fig. 2.18. This figure also shows the rack dimensions, namely, $\bar{a}$ the clear spacing of the rack bars, $\bar{b}$ the center to center bar spacing and $\bar{L}$ and $\bar{d}$ the width and the thickness of the bars, respectively.

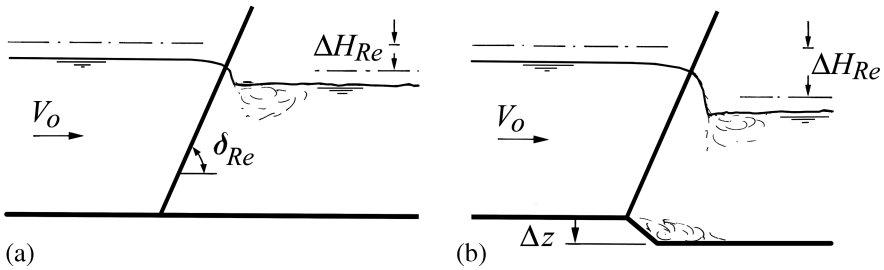

Fig. 2.17 Rack (schematic) in open channel (**a**) without and (**b**) *with* depressed downstream floor

Table 2.7 Rack factor β_{Re} in relation to the rack geometry shown in Fig. 2.18

Type	1	2	3	4	5	6	7
β_{Re}	1	0.76	0.76	0.43	0.37	0.30	0.74

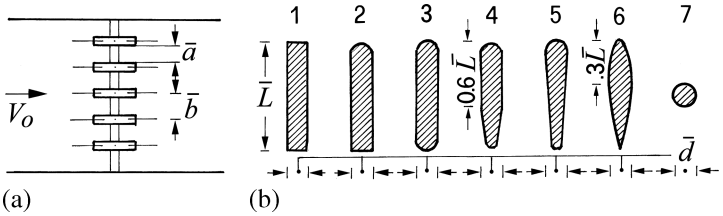

Fig. 2.18 (**a**) Plan of the rack bars, (**b**) Types of rack bars

For *clean racks* $c_{Re} = 1$, for mechanically cleaned racks c_{Re} varies between 1.1 and 1.3 and for the manually cleaned racks c_{Re} varies between 1.5 and 2. The rack geometry enters with the factor ζ_{Re} (Idel'cik 1979). Customarily, ζ_{Re} amounts to around 1. In the following, a simplified procedure is presented.

Equation (2.46) simplifies if the ratio $\bar{L}/\bar{d}$ equals to about 5 and $\bar{a}/\bar{b} > 0.5$, i.e. the rack bars are slender. Then, according to Idel'cik (1979)

$$\xi_{Re} = \frac{7}{3}\beta_{Re}c_{Re}\left[\frac{\bar{b}}{\bar{a}} - 1\right]^{4/3} \sin\delta_{Re}. \tag{2.47}$$

For rough estimates of the rackloss, *ad hoc* values of 5 cm for mechanically cleaned racks and a maximum of 10 cm for manually cleaned racks are adopted for a velocity of around 1 ms^{-1}. To compensate for the head loss $\Delta H_{Re} = \xi_{Re} \cdot V_o^2/(2g)$, the channel floor downstream of the rack is often depressed by the amount $\Delta z = \Delta H_{Re}$ (Fig. 2.17b).

2.3.9 *Slide Gate*

Slide gates (German: Plattenschieber; French: Vanne à tiroir) are installed in pressure conduits either fixed or adjustable in position. Figure 2.19 shows three main types with a) straight bottomed closing edge, b) semi-circular bottom geometry of radius R_s as well as c) with a guide ring. Let the conduit diameter be D and the axial opening height s. Further, let r_v be the rounding radius of the bottom edge and t_p the gate thickness (Fig. 2.19d).

In the following the customary circular sharp-edged slide gate of cross-sectional area $F_o = \pi D^2/4$ and with a semi-circular bottom edge of relative diameter $2R_s/D \cong 1.2$ are considered. The relations between the relative cross-sectional area F/F_o and the gate opening factor $S = s/D$ are then approximately

$$\text{Straight bottom edge} \quad F/F_o = 1.70S^{3/2}\left[1 - \frac{1}{4}S - \frac{4}{25}S^2\right], \tag{2.48}$$

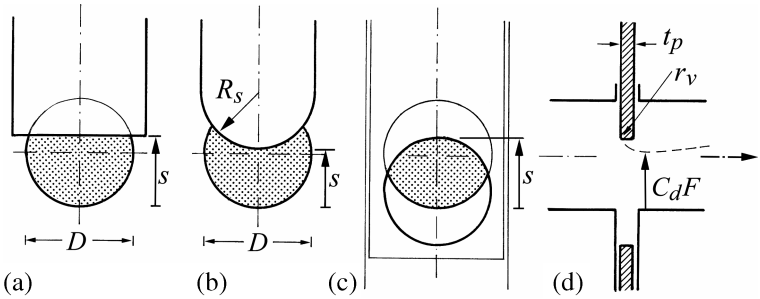

Fig. 2.19 Slide gate, definition sketches for (**a**) straight bottom gate, (**b**) semi-circular bottom geometry, (**c**) gate with guide ring, (**d**) streamwise flow pattern

$$\text{Semi-circular bottom edge} \quad F/F_o = 1.20S\left[1 - \frac{1}{6}S^3\right], \tag{2.49}$$

$$\text{With ring guide} \quad F/F_o = S^{4/3}. \tag{2.50}$$

Experimental studies by Schedelberger (1975) show that the contraction coefficient C_d (Fig. 2.19d) and the corresponding loss coefficient ξ_p depend only on the edge rounding radius r_v and the area ratio $\phi = F/F_o$. In contrast, no effects neither of the relative gate thickness t_p/D, nor of the gate shape or even of the Reynolds number $\mathsf{R} = V_oD/v$ in the downstream conduit are detected. The test results are characterized by the minimum (subscript o) value

$$C_{do} = 0.61 + \frac{2}{3}\rho_p^{1/2}, \tag{2.51}$$

where $\rho_p = r_v/D \leq 0.2$ is the degree of edge rounding. For $\rho_p = 0$, Eq. (2.51) yields the basic contraction ratio 0.61. The dependence of the *coefficient of discharge* C_d on the area ratio ϕ follows the relation

$$C_d = C_{do} + 0.73\left[\phi - \frac{2}{3}\rho_p^{1/7}\right]^2. \tag{2.52}$$

For $\phi = 1$ all values of C_d tend eventually to unity.

The *loss coefficient* $\xi_p = \Delta H/\left[V_o^2/(2g)\right]$ expressed in terms of the approach flow velocity $V_o = Q/(\pi D^2/4)$ follows the modified Borda-Carnot relation

$$\xi_p = \left[\frac{1}{C_d\phi} - 1\right]^2. \tag{2.53}$$

This is true only for pressurized flow. For *free surface flow* $\xi_p = 0$, potential flow prevails, and the *discharge* Q is with Eq. (2.52)

$$Q = C_d F[2g(h_o - h_u)]^{1/2}, \tag{2.54}$$

where h_o is the upstream pressure head and h_u the mean downstream flow depth. Often h_u is negligible as compared to h_o. An alternative derivation is presented in Chap. 4.

2.4 Discussion of Results

2.4.1 *Free Surface and Pressurized Flows*

The preceding discussion concerning the additional losses involves primarily *pressurized conduit flow* (German: Druckrohrabfluss; French: Ecoulement en charge). The influence of the free surface is discussed here because pressurized conduit flow can be regarded as a special case with the Froude number (Chap. 6) tending to zero.

The results on loss coefficients pertain only to important cases of sewer flow. There exists, however, an enormous amount of data on loss coefficients which have been lucidly summarized, for example, by Idel'cik (1979), Blevins (1984) or Miller (1994). The flow elements mentioned here are explained with reference to pressurized conduits but can be applied also for *free surface flows* (German: Freispiegelabfluss; French: Ecoulement à surface libre). For example, bend or junction elements are frequently met in sewer systems. The dominant emphasis in the available data relates to pressurized conduits whereas relatively few studies with the corresponding open channel flow have been undertaken. The question therefore arises as to whether it is possible to transform the loss values obtained in pressurized conduits to comparable flow situations in free surface channels and, if so, what limits restrict their applicability?

To answer these questions, first the equations of closed conduit and free surface flows are established. For this purpose, the energy line slope is designated S_E and the slope of the conduit axis on the channel bed is designated S_o. With $h_p = p/(\rho g)$ as the pressure head, the system of equations for the *pressurized conduit* at location $x = x^*$ is (Fig. 2.20)

$$H = h_p + \frac{V^2}{2g}, \quad \frac{\mathrm{d}H}{\mathrm{d}x} = S_o - S_E, \tag{2.55}$$

and for the *free-surface channel* with the water depth h

$$H = h + \frac{V^2}{2g}, \quad \frac{\mathrm{d}H}{\mathrm{d}x} = S_o - S_E. \tag{2.56}$$

The *cross-sectional area* F of a pressure conduit is given by $F = F(x)$ thereby accounting for the cross-sectional variation along the direction of flow (Fig. 2.20a).

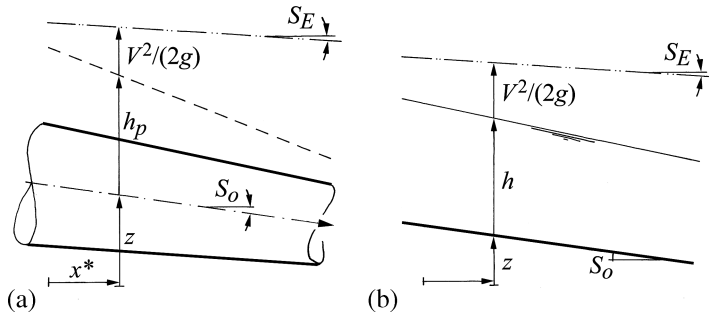

Fig. 2.20 Similarity between flow in (**a**) pressurized conduit and (**b**) free-surface channel

For a free-surface channel, the cross-sectional area F at a section $x = x^*$ can vary with both the local water depth h *and* the distance along the channel, expressed as $F = F(x,h)$. If V is set equal to Q/F in Eqs. (2.55) and (2.56), and the equations are then differentiated with respect to x assuming constant discharge Q, it follows for *pressurized conduit flow*

$$\frac{\mathrm{d}h_p}{\mathrm{d}x} - \frac{Q^2}{gF^3}\frac{\mathrm{d}F}{\mathrm{d}x} = S_o - S_E, \tag{2.57}$$

and for *free-surface flow*

$$\frac{\mathrm{d}h}{\mathrm{d}x} - \frac{Q^2}{gF^3}\frac{\mathrm{d}F}{\mathrm{d}x} = S_o - S_E. \tag{2.58}$$

For given conduit geometry, including area function $F(x)$, inclination of the conduit axis $S_o(x)$ as well as known discharge Q and friction slope S_E, Eq. (2.57) can be solved for the local pressure head function $h_p(x)$. In contrast, the solution of Eq. (2.58) needs further development. Given that the *total derivative* of a function $F = F(x,h)$ equals

$$\frac{\mathrm{d}F}{\mathrm{d}x} = \frac{\partial F}{\partial x} + \frac{\partial F}{\partial h}\cdot\frac{\mathrm{d}h}{\mathrm{d}x} \tag{2.59}$$

the analogy to Eq. (2.58) is

$$\frac{\mathrm{d}h}{\mathrm{d}x}[1 - \mathsf{F}^2] - \frac{Q^2}{gF^3}\frac{\partial F}{\partial x} = S_o - S_E. \tag{2.60}$$

The similarity of Eqs. (2.57) and (2.60) shows that pressurized and free-surface flows are identical provided $\mathsf{F}^2 = Q^2/(gF^3)(\partial F/\partial h) = 0$, i.e. if the *Froude number* (German: Froudezahl; French: Nombre de Froude) equals zero. As discussed in Chap. 6, the dimensionless number F characterizes the dynamics of free-surface

flows. From the preceding derivations it is now clear that pressurized flow represents a special case of free-surface flow and that the loss coefficients (obtained for pressurized flows) can be carried over to the corresponding open channel flow situation provided the Froude number remains small. The absolute upper limit is $\mathsf{F} = 1$, i.e. so-called critical flow, for which the pressure term in Eq. (2.60) completely vanishes. In practice, the transformation concept of the loss coefficients to free-surface channels can be applied up to about $\mathsf{F} = 0.7$. Beyond this value, this simplified concept ceases to be valid owing to streamline curvature effects in the form of *standing surface waves* (Chap. 1).

2.4.2 *Transformation Principle*

The preceding observation that the loss coefficients determined for pressure conduits may also be applied to open channel flow is of practical importance. Were this not so, many extensive series of investigations would have to be repeated with the additional parameter F. Various studies point to the transferability of the loss coefficients. In practice, this calculation procedure has been in use for a long time primarily because of the absence of any other data basis. A proof was however still lacking. If the *transformation principle* from pressurized to free-surface flows is accepted, solutions of many engineering problems are sufficiently accurate. This is verified in Chap. 16 for the selected example of junction manholes.

At this point a further proposition may be introduced for which the derivations that follow are essentially simple. Starting from the notion of energy head

$$H = z + h + \frac{Q^2}{2gF^2} \tag{2.61}$$

pertaining to a cross-section at location $x = x^*$ (Fig. 2.21) and denoting the average slope of the energy line S_E the following holds for two adjacent cross-sections ① and ②

$$z_1 + h_1 + \frac{Q_1^2}{2gF_1^2} = z_2 + h_2 + \frac{Q_2^2}{2gF_2^2} + S_E L_{12}. \tag{2.62}$$

The *energy loss* $\Delta H_{12} = S_E L_{12}$ is set equal to the sum of the friction loss $\Delta H_R = S_f L_{12}$ and the additional loss $\Delta H_L = \xi_{12}(V_1^2/2g)$ If the bottom slope is S_o, the bottom level difference $(z_1 – z_2) = S_o L_{12}$, then (Fig. 2.21)

$$(S_o - S_f)L_{12} = h_2 - h_1 + \frac{Q_2^2}{2gF_2^2} - \frac{Q_1^2}{2gF_1^2}(1 - \xi_{12}). \tag{2.63}$$

Equation (2.63) is the basic equation for calculating *water surface profiles* over an element of length L_{12} with additional losses included. For subcritical flow, the

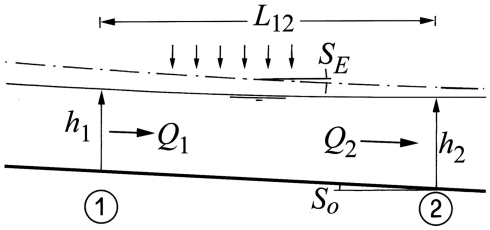

Fig. 2.21 Flow in open channel with hydraulic losses

parameters at the downstream cross-section ② are known, and those in the upstream cross-section ① are sought (Chap. 8). The upstream flow depth h_1 can therefore be determined from Eq. (2.63) provided the channel geometry is defined.

Subcritical flows ($\mathsf{F} < 1$) are characterized by a large static pressure portion h and a relatively small dynamic portion $V^2/2g$. The energy head with respect to the channel bottom is

$$H_* = H(z = 0) = h + \frac{Q^2}{2gF^2}. \tag{2.64}$$

For so-called *weak* subcritical flows ($\mathsf{F} < 0.5$) that are of primary concern here, one gets $Q^2/(2gF^2h) << 1$. Accordingly, by an approximate method the dynamic portion is slightly modified. The calculation is simplified significantly if assuming a constant velocity head over the length L_{12}. This transforms Eq. (2.63) to

$$h_1 - h_2 = (S_o - S_f)L_{12} - \frac{Q_2^2}{2gF_2^2}\xi_{12}. \tag{2.65}$$

This relation gives explicitly the unknown upstream flow depth h_1 if the average friction slope $S_{fa} = (S_{f1}+S_{f2})/2$ is replaced by the *constant* energy line slope $S_f = S_{f2}$, and

$$h_1 - h_2 = (S_o - S_{f2})L_{12} - \frac{Q_2^2}{2gF_2^2}\xi_{12}. \tag{2.66}$$

This last simplification is again valid since the energy gradient strongly depends on the Froude number and tends to zero for small values of F. Besides, the length L_{12} is often small in comparison with a typical length and consequently the friction effect is not significant. Equation (2.66) possesses a form convenient for practical calculations and allows *explicit* determination of flow depth h_1 in the upstream cross-section. For a channel in which the friction gradient S_f is nearly compensated for by the bottom slope S_o, Eq. (2.66) reduces to

$$h_1 = h_2 + \frac{Q_2^2}{2gF_2^2}\xi_{12}. \tag{2.67}$$

Channels which satisfy the condition $S_o = S_f$ are often found in practice, because the friction gradient S_f normally lies between 0.1% and 1%. Eq. (2.67) emphasizes that the upstream flow depth h_1 then equals the downstream flow depth h_2 plus the product of the loss coefficient ξ_{12} and velocity head $V_2^2/(2g)$. Applications of these relations are discussed subsequently.

Notation

$\bar{a}$	[m]	clear spacing of rack bars
$\bar{b}$	[m]	centre to centre spacing of rack bars
c_{Re}	[–]	coefficient for rack logging
c_w	[–]	resistance coefficient
C_d	[–]	coefficient of discharge
$\bar{d}$	[m]	thickness of rack bars
D	[m]	diameter
D_o	[m]	diameter relative to S_f and D
D^*	[–]	non-dimensional diameter relative to D_o
f	[–]	friction factor
F	[m^2]	cross-sectional area
F	[–]	Froude number
g	[ms^{-2}]	acceleration due to gravity
h	[m]	flow depth
h_p	[m]	pressure head
H	[m]	energy head
k_s	[m]	equivalent sand roughness height
k_s^*	[–]	sand roughness relative to D_o
$\bar{L}$	[m]	length of rack bars
L_k	[m]	length of bend
L_{12}	[m]	distance between two cross-sections
m	[–]	area ratio for conduit junction (combining flow)
n	[–]	area ratio for conduit junction (combining flow)
$1/n$	[$m^{1/3}s^{-1}$]	roughness coefficient
N	[–]	viscosity parameter
p	[Nm^{-2}]	pressure
$\bar{p}$	[Nm^{-2}]	mean pressure
p'	[Nm^{-2}]	fluctuating pressure component
p_d	[Nm^{-2}]	dynamic pressure
p_g	[Nm^{-2}]	total pressure
p_s	[Nm^{-2}]	static pressure
q	[–]	discharge ratio for conduit junction (combining flow)
$\hat{q}$	[–]	relative discharge
Q	[m^3s^{-1}]	discharge

Q_o	[m^3s^{-1}]	discharge normalized with S_f and D
r_v	[m]	radius of rounding
R	[m]	centre line radius of conduit bend
R_s	[m]	radius of semi-circular bottom gate
R	[–]	Reynolds number
s	[m]	height of gate opening
S	[–]	gate opening ratio
S_E	[–]	energy gradient
S_f	[–]	friction gradient
S_o	[–]	bottom slope
t	[s]	time
t_p	[m]	gate thickness
T	[–]	turbulence number
V	[ms^{-1}]	average velocity
x	[m]	length coordinate
z	[m]	elevation coordinate
β_{Re}	[–]	rack coefficient
δ	[–]	angle
δ_{Re}	[–]	rack angle
ε	[–]	relative wall roughness height
ϕ	[–]	area ratio
Φ_e	[–]	influence of expansion angle
μ	[–]	velocity ratio
ν	[m^2s^{-1}]	kinematic viscosity
ν^*	[–]	viscosity relative to D_o and Q
ρ	[kgm^{-3}]	density
ρ_p	[–]	degree of rounding
ξ	[–]	loss coefficient
ξ_{12}	[–]	loss coefficient between two cross-sections
ζ_{Re}	[–]	rack coefficient
Ξ	[–]	ratio of loss coefficients

Subscripts

a	lateral outflow branch
d	through branch
e	expansion
g	total, sum
k	bend
L	additional, local
m	minimum
o	lateral branch, approach flow
opt	optimum

p	slide plate (gate)
R	friction
r	rough
Re	rack
s	smooth
t	transition
T_t	T-piece, flow division
T_v	T-piece, combining flow
tot	total
u	downstream branch
v	contraction
z	lateral inflow
1	inflow
2	outflow

References

American Society of Civil Engineers ASCE (1969). Design and construction of sanitary and storm sewers. *Manuals and Reports of Civil Engineering Practise* 37. ASCE: New York.

Benedict, R.P., Carlucci, N.A., Swetz, S.D. (1966). Flow loss in abrupt enlargements and contractions. *Journal of Engineering for Power* 88(1): 73–81.

Blevins, R.D. (1984). *Applied fluid dynamics handbook*. Van Nostrand Reinhold: New York.

Chen, J.J.J. (1985). Systematic explicit solutions of the Prandtl and Colebrook-White equations for pipe flow. *Proc. Institution Civil Engineers* 79: 383–389; 81: 159–165.

Chow, V.T. (1959). *Open channel hydraulics*. McGraw-Hill: New York.

Eck, B. (1991). *Technische Strömungslehre* (Technical fluid flow). 9th edition. Springer: Berlin [in German].

Favre, H. (1937). Sur les lois régissant le mouvement des fluides dans les conduites en charge avec adduction latéral (On the laws governing the fluid motion in pressurized conduits with lateral discharge). *Revue Universelle des Mines* 80: 502–512 [in French].

Gardel, A. (1957). Les pertes de charge dans les écoulements au travers de branchements en té (The head losses for flows in T-junctions). *Bulletin Technique de la Suisse Romande* 83(9): 123–130; 83(10): 143–148 [in French].

Gardel, A. (1962). Perte de charge dans un étranglement conique. (Head loss in a conical contraction). *Bulletin Technique de la Suisse Romande* 88(21): 313–320; 88(22): 325–337 [in French].

Gardel, A., Rechsteiner, G.F. (1970). Les pertes de charge dans les branchements en té des conduites de section circulaire (Head losses in T-junctions of circular conduits). *Bulletin Technique de la Suisse Romande* 96(25): 363–391 [in French].

Hager, W.H. (1984). An approximate treatment of flow in branches and bends. *Proc. Institution of Mechanical Engineers* 198C(4): 63–69.

Hager, W.H. (1987). Die Berechnung turbulenter Rohrströmungen (The computation of turbulent pipe flows). 3*R-International* 26(2): 116–121 [in German].

Hager, W.H. (1990). Strömungsverhältnisse in Rohr- und Kanal-Erweiterungen (Flow patterns in pipe and channel expansions) *Österreichische Wasserwirtschaft* 42(11/12): 305–312 [in German].

Hager, W.H. (1992). Kniekrümmer (Mitre bends). 3*R-International* 32(2/3): 94–100 [in German].

Idel'cik, I.E. (1979). *Memento des pertes de charge* (Handbook of energy losses) 2nd edition. Eyrolles: Paris [in French].

Idel'cik, I.E. (1986). *Handbook of hydraulic resistance*. Hemisphere Publishing Corporation: Washington.

Ito, H. (1960). Pressure losses in smooth pipe bends. *Journal of Basic Engineering* 82: 131–143.

Ito, H., Imai, K. (1973). Energy losses at 90° pipe junctions. *Journal of the Hydraulics Division* ASCE 99(HY9): 1353–1368; 100(HY8): 1183–1185; 100(HY9): 1281–1283; 100(HY100): 1491–1493; 101(HY6): 772–774.

Knapp, F.H. (1960). *Ausfluss, Überfall und Durchfluss im Wasserbau* (Outflow, overflow and throughflow in hydraulic structures). G. Braun: Karlsruhe [in German].

Miller, D.S. (1971). *Internal flow*. BHRA: Cranfield-Bedford.

Miller, D.S. (1978). *Internal flow systems*. BHRA Fluid Engineering: Cranfield-Bedford.

Miller, D.S., ed. (1994). *Discharge characteristics*. IAHR Hydraulic Structures Design Manual 8. Balkema: Rotterdam.

Naudascher, E. (1987). *Hydraulik der Gerinne und Gerinnebauwerke* (Hydraulics of channels and channel structures). Springer: Wien, New York [in German].

Richter, H. (1971). *Rohrhydraulik* (Pipe hydraulics). Springer: Berlin [in German].

Schedelberger, J. (1975). Schliesscharakteristiken von Einplattenschiebern (Closing characteristics of singular plate gates). 3*R-International* 14(3): 174–177 [in German].

Schröder, R.C.M. (1990). Hydraulische Methoden zur Erfassung von Rauheiten (Hydraulic methods for the definition of roughnesses). *DVWK Schrift* 92. Parey: Hamburg, Berlin [in German].

Sinniger, R.O., Hager, W.H. (1989). *Constructions hydrauliques – Ecoulements stationnaires* (Hydraulic structures – steady flows). Presses Polytechniques Romandes: Lausanne [in French].

Vischer, D. (1958). Die zusätzlichen Verluste bei Stromvereinigung in Druckleitungen (The additional losses due to junction flow in pipes). *Dissertation* TH Karlsruhe, appeared also as *Arbeit* 147, Th. Rehbock-Laboratorium: Karlsruhe [in German].

Ward-Smith, A.I. (1980). *Internal fluid flow*. Clarendon Press: Oxford.

Zigrang, D.J., Sylvester, N.D. (1985). Discussion to "A simple explicit formula for the estimation of pipe friction factor", by J.J.J. Chen. *Proc. Institution Civil Engineers* 79: 218–219.

http://www.springer.com/978-3-642-11382-6

Wastewater Hydraulics
Theory and Practice
Hager, W.H.
2010, XX, 652 p., Hardcover
ISBN: 978-3-642-11382-6